


**Spontaneous emission in nanofibers doped with an ensemble of quantum dots and quantum emitters**Mahi R. Singh ,\* Grant Brassem , and Patrick D. Persaud *Department of Physics and Astronomy, The University of Western Ontario, London, Ontario, Canada N6A 3K7*

(Received 10 September 2020; accepted 12 November 2020; published 4 December 2020)

We studied the effect of the spontaneous emission on the photoluminescence (PL) of photonic nanofibers doped with an ensemble of quantum dots (QDs) and quantum emitters. Quantum emitters can be molecular dyes or DNA molecules. Bound photonic states of the nanofiber hybrid are calculated using the transfer-matrix method based on the Maxwell equations. It is shown that the number of bound states in the nanofiber hybrid depends on the size and shape of the nanofiber along with the concentration of quantum dots and quantum emitters including their dielectric constants. The bound photon electric field induces dipoles in quantum dots and quantum emitters, and they interact with each other via the dipole-dipole interaction (DDI). We found that excited excitons decay spontaneously due to the interaction between excitons and the DDI field. It is found that the decay linewidth is enhanced when the bound photon energy is close to the exciton energy. On the other hand, we predicted that in the weak DDI coupling limit and when the bound photon energy is far away from the exciton energy the decay linewidths are suppressed (quenched). An analytical expression of the photoluminescence is found using the density-matrix method in the presence of the DDI coupling. We have predicted that in the strong DDI coupling limit the peak in the photoluminescence spectrum splits into two peaks when the bound photon energy is far away from the exciton energy. Furthermore, we have shown that when the bound photon energy is close to the exciton energy, two peaks merge into one peak. We have also compared our theory with PL experiments of a nanofiber doped with an ensemble of the CdSe QDs and sulforhodamine 101 dye molecules. A good agreement between theory and experiments is found. Our theory can be used by experimentalists to perform alternative types of experiments and for fabricating types of nanosensors and nanoswitches.

DOI: [10.1103/PhysRevA.102.063704](https://doi.org/10.1103/PhysRevA.102.063704)**I. INTRODUCTION**

Recently there is considerable interest to study the optical properties of nanofibers doped with an ensemble of quantum dots (QDs) [1–12]. For example, Wang *et al.* [1] fabricated poly-phenylenevinylene nanofibers via the electrospinning method and introduced an ensemble of CdS QDs inside nanofibers. The QDs were distributed in the fibers evenly and the surface of fibers was very smooth. They concluded that this kind of nanohybrid material has tunable fluorescence properties and will have potential applications for optical and electric devices. Further, Cheng *et al.* [2] have studied the photoluminescence (PL) in the PbSe-QD doped fiber amplifier based on the sodium-aluminum-borosilicate-silicate glass. They found photoluminescence emission is strong and stable in the near-infrared region. Zhang *et al.* [3] found an enhanced ultraviolet emission from highly dispersed ZnO QDs embedded in poly(vinyl pyrrolidone) electrospun nanofibers.

Additionally, Strong *et al.* [4] fabricated highly crystalline, doped polythiophene from the surfaces of CdTe quantum dots by ligand exchange of 3-thenoic acid followed by an oxidant-initiated polymerization. This produced a composite of highly ordered nanofibers, which transferred charge efficiently between the polythiophene and the quantum dots. Camposeo *et al.* [5] examined properties and applications of

electrospun light-emitting nanofibers, as well as manufacturing techniques. The applications include nanoscale organic light-emitting diodes and optically pumped lasers, field-effect transistors, and high-performance optical sensors, among others.

De San Luis *et al.* [6] studied hybrid nanofibers containing CdSe/ZnS quantum dots. They have been produced by electrospinning of hybrid latexes, synthesized by seeded semi-batch emulsion polymerization, thereby creating cross-linked core-shell polystyrene (PS)–QD–Poly (methyl methacrylate) particles. The hybrid nanofibers are sensitive to selected solvents and are good candidates to produce volatile organic compound sensors. Additionally, Fahmi *et al.* [7] examined the directed self-assembly of one-dimensional hybrid materials based on a poly(propyleneimine) dendrimer template and CdSe nanoparticles. This can be used to form semiconducting hybrid nanofibers coated with discrete Au nanoparticles. Such nanofibers have potential in various applications, such as biological markers and nanoprobe. Camposeo *et al.* [8] studied the fabrication via electrospinning of polymer nanofibers in order to better control both surface properties and geometry. They examined the spectroscopy of light emitted by molecular compounds and single quantum dots embedded in these polymer fibers.

Next, Abitbol *et al.* [9] fabricated fluorescent cellulose triacetate fibers by electrospinning solutions of methylene chloride and methanol which contained CdSe/ZnS QDs. This resulted in fluorescent fibers that were not significantly

\*msingh@uwo.ca

altered by the nanoparticles, with generally smooth surfaces. Yan *et al.* [10] studied a cellulose nanofiber embedded with cadmium sulfide quantum dots. This nanohybrid exhibits 95% light transmittance at 550 nm. Chaguetmi *et al.* [11] developed a new type of nanostructure for photo-electrochemical water splitting, based on scheduled CdS-TiO<sub>2</sub> nanocomposite films. TiO<sub>2</sub> nanofibers are created using controlled corrosion of polished Ti sheets and the direct embedding of TiO<sub>2</sub>-Ti sheets by CdS quantum dots. A net enhancement of the photocurrent was observed in the presence of CdS QDs.

Recently, Singh *et al.* [12] have fabricated nanofibers embedding an ensemble of CdSe QDs and sulforhodamine 101 (S101) dye molecules, via the self-assembly process of a polystyrene-block-poly(4-vinylpyridine) (PS-*b*-P4VP) block copolymer. The cylindrical domains subsequently were isolated as individual nanofibers via the selective-swelling approach. The confinement imposed due to the nano-dimension geometry of the cylindrical nanofibers enabled the QDs and S101 dyes to interact with each other. They measured the photoluminescence spectrum of the CdSe QD by embedding a different concentration of S101 dye molecules. They found that the PL spectrum split from one peak to two peaks by increasing the concentration of dye molecules.

In this paper, we studied the effect of the spontaneous emission on the PL of photonic nanofibers doped with an ensemble of quantum dots and quantum emitters (QEs). We call this combined system a nanofiber hybrid (NFH). The quantum emitters can be molecular dye molecules or DNA molecules. Bound photons in the nanofiber induce dipoles in the QDs and QEs. Therefore, QDs and QEs interact with each other via the dipole-dipole interaction (DDI). An analytical expression of the PL is obtained by using the density-matrix method. Recently, there is considerable interest to apply the density-matrix method in quantum dot nanohybrids [13–23].

In Sec. I, we surveyed the literature for nanofiber hybrids. In Sec. II, a theory of the light propagation in the NFH is developed. To calculate the bound photonic states, we used the transfer-matrix method of the Maxwell equations. In Sec. III, a theory of spontaneous decay linewidths due to the exciton-DDI coupling is developed using the time-dependent quantum-mechanical perturbation method. The density of states (DOS) for the bound photon in the NFH is evaluated. Analytical expressions of the decay linewidths are also obtained. In Sec. IV, an analytical expression of the PL is derived using the density-matrix method. In Sec. V, we have performed numerical calculations for the spontaneous decay linewidths. Next, we have compared our theory with the PL experiments from Ref. [12]. Finally, we have summarized the findings of our paper in Sec. VI.

## II. THE BOUND PHOTONIC STATES IN NANOFIBER HYBRIDS

In this section, we calculate the bound photonic states in the nanofiber hybrid. We consider a nanofiber made of a core dielectric material and a shell (cladding) dielectric material. It is called the core-shell nanofiber. The cross-sectional area of the core is denoted as  $A$  and the length of the nanofiber is  $L$ . The typical diameter of the nanofiber lies between 50 and 500 nm. The core of the nanofiber is doped with an ensemble

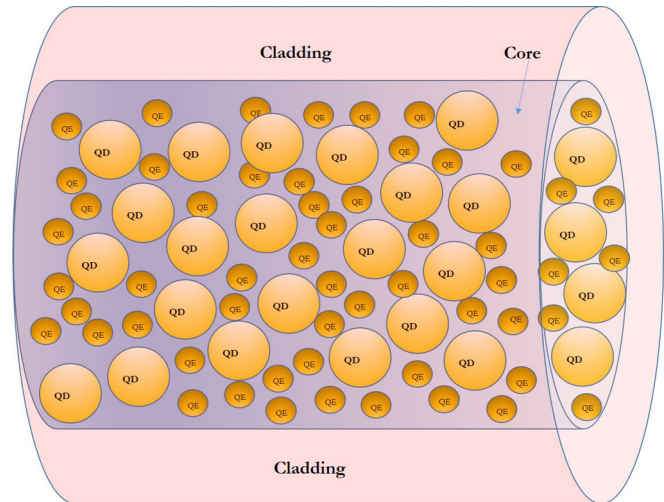


FIG. 1. A schematic diagram of the nanofiber hybrid is plotted. The nanofiber is made of a core dielectric material and a shell (cladding) dielectric material. The core of the nanofiber is doped with an ensemble of QDs and QEs.

of QDs and QEs which are densely populated in the core-shell nanofiber. This nanofiber hybrid lies along the  $z$  direction. A schematic diagram of the nanofiber hybrid is shown in Fig. 1.

A probe electromagnetic field with amplitude  $\mathbf{E}_p$ , photon energy  $\varepsilon_k$ , and wave vector  $k$  is applied to study the photoluminescence and it is expressed as

$$\mathbf{E}_{\text{probe}} = \mathbf{E}_p e^{i(k \cdot r - \varepsilon_k t / \hbar)}. \quad (1)$$

The probe photon field propagates along the length direction (i.e.,  $z$  direction) of the NFH and is confined in a perpendicular direction (i.e.,  $x$ - $y$  directions) in the NFH. Due to the confinement of the electric field perpendicular to the nanofiber, the probe photon energies are quantized.

Now, let us calculate the propagation of the electric field inside the NFH. The electric field inside the core propagate freely along the  $z$  direction and it exponentially decays in the shell. The dielectric constant of the core is found as

$$\varepsilon_c = n_{\text{QE}} \varepsilon_{\text{QE}} + n_{\text{QD}} \varepsilon_{\text{QD}} + \varepsilon_b, \quad (2)$$

where  $n_{\text{QE}}$  and  $n_{\text{QD}}$  are the concentration ratios of the QEs and QDs, respectively. Here  $\varepsilon_{\text{QE}}$  and  $\varepsilon_{\text{QD}}$  are the dielectric constants of the QE and QD, respectively. Here  $\varepsilon_b$  is the dielectric constant of the core background material.

The dispersion relation between the wave vector  $k$  and energy  $\varepsilon_k$  is written as

$$\varepsilon_k = \left( \frac{\hbar c}{\sqrt{(n_{\text{QE}} \varepsilon_{\text{QE}} + n_{\text{QD}} \varepsilon_{\text{QD}} + \varepsilon_b)}} \right) k, \quad (3)$$

where  $c$  is the speed of light in the vacuum. Equation (3) can be rewritten in the following form:

$$k_x^2 + k_y^2 + k_z^2 = F_c^2(\varepsilon_k), \quad (4)$$

$$F_c(\varepsilon_k) = \frac{\varepsilon_k \sqrt{(n_{\text{QE}} \varepsilon_{\text{QE}} + n_{\text{QD}} \varepsilon_{\text{QD}} + \varepsilon_b)}}{\hbar c},$$

where  $k_x$ ,  $k_y$ , and  $k_z$  are the components of wave vector  $k$  propagating along  $x$ ,  $y$ , and  $z$  directions, respectively.

Similarly, the dispersion relation for the electric field in the shell of the nanofiber is written as

$$q_x^2 + q_y^2 + q_z^2 = F_s^2(\varepsilon_q), \quad (5)$$

$$F_s(\varepsilon_q) = \frac{\varepsilon_q \sqrt{\varepsilon_s}}{\hbar c},$$

where  $\varepsilon_s$  is the dielectric constant of the shell, and  $\varepsilon_q$  is the photon energy for the wave vector  $q$ . Here  $q_x$  and  $q_y$  are the components of the decaying wave vector  $q$  along  $x$  and  $y$  directions, respectively, and  $q_z = k_z$ , where  $k_z$  is the propagating wave vector along the  $z$  direction.

We know that the electric field propagates along with the core and it exponentially decays in the shell. Therefore, matching the boundary conditions at the interface between the core and shell and using the transfer-matrix method based on the Maxwell equations [24,25], we get the following

$$F_x = 0, \quad F_x = k_x F_s^2(\varepsilon_k) \tan(k_x d_x / 2 - n\pi / 2) - F_c^2(\varepsilon_k) [F_c^2(\varepsilon_k) - F_s^2(\varepsilon_k) - k_x^2]^{1/2},$$

$$F_y = 0, \quad F_y = k_y F_s^2(\varepsilon_k) \tan(k_y d_y / 2 - m\pi / 2) - F_c^2(\varepsilon_k) [F_c^2(\varepsilon_k) - F_s^2(\varepsilon_k) - k_y^2]^{1/2}. \quad (8)$$

Note that  $F_x$  and  $F_y$  are the functions of  $k_x$  and  $k_y$ , respectively. Hence, the quantized (bound) photon energies can be calculated for given quantum numbers  $n$  and  $m$  by solving Eq. (8) self-consistently for  $k_x$  and  $k_y$ . We denote  $k_x$  and  $k_y$  as  $k_n$  and  $k_m$ , respectively. Let us denote the bound photon energy in the  $x$ - $y$  direction as  $\varepsilon_{nm}$ . Therefore,  $\varepsilon_{nm}$  is calculated from Eq. (4) by putting  $k_z = 0$  and we get

$$k_n^2 + k_m^2 = F_c^2(\varepsilon_{nm}, k_z = 0) = F_c^2(\varepsilon_{nm}). \quad (9)$$

It is important to note that the bound-state energy  $\varepsilon_{nm}$  depends on the function  $F_c$  which in turn depends on the dielectric constants of the core material, the concentration of the QDs, and QEs along with their dielectric constants.

Now the wave vector and energy of the electric field propagating inside the NFH are expressed as  $k_{nm,z} = (k_n, k_m, k_z)$  and energy  $\varepsilon_{nm,z}$ , respectively. The dispersion relation for the electric field inside the NFH can be found from Eq. (4) by replacing  $k$  by  $k_{nm,z}$  and  $\varepsilon_k$  by  $\varepsilon_{nm,z}$  and it can be expressed as

$$k_n^2 + k_m^2 + k_z^2 = F_c^2(\varepsilon_{nm,k_z}). \quad (10)$$

Further, we can simplify the expression of the dispersion relation by substituting Eq. (9) into Eq. (10) and we get

$$k_z = [F_c^2(\varepsilon_{nm,k_z}) - F_c^2(\varepsilon_{nm})]^{1/2}. \quad (11)$$

The above dispersion relation will be used to calculate the DOS of bound photons propagating inside the nanofiber. We show in the next section that the spontaneous decay linewidths of excitons in the QD depend on the DOS of bound photons.

### III. FORMULATION OF THE BOUND STATES AND LINEWIDTHS IN NANOFIBER HYBRIDS

In this section, we investigate the effect of bound states in the decay linewidths of excitons in the QD. We consider that the QD has three energy levels and they are denoted as

bound-state energies in the nanofiber:

$$k_x F_s^2(\varepsilon_k) \sin(k_x d_x - n\pi / 2) - q_x F_c^2(\varepsilon_k) \cos(k_x d_x - n\pi / 2) = 0,$$

$$k_y F_s^2(\varepsilon_k) \sin(k_y d_y - m\pi / 2) - q_y F_c^2(\varepsilon_k) \cos(k_y d_y - m\pi / 2) = 0, \quad (6)$$

where

$$q_x = [F_c^2(\varepsilon_k) - F_s^2(\varepsilon_k) - k_x^2]^{1/2},$$

$$q_y = [F_c^2(\varepsilon_k) - F_s^2(\varepsilon_k) - k_y^2]^{1/2}. \quad (7)$$

Here  $d_x$  and  $d_y$  are the diameter of the core along the  $x$  direction and  $y$  direction, respectively. Here  $n$  and  $m$  are the quantum numbers.

Inserting Eq. (7) into Eq. (6), we get

$|1\rangle$ ,  $|2\rangle$ , and  $|3\rangle$ . These types of QDs are called three-level quantum systems. The energy difference between  $|1\rangle$  and  $|2\rangle$  is expressed as  $\varepsilon_{21}$ . Similarly, the energy difference between  $|2\rangle$  and  $|3\rangle$  is expressed as  $\varepsilon_{23}$ . Therefore, the energy difference between levels  $|1\rangle$  and  $|3\rangle$  is found as  $\varepsilon_{311} = \varepsilon_{21} - \varepsilon_{23}$ . A schematic diagram of the QD is shown in Fig. 2.

To study the decay linewidth, we need to calculate how many electric fields are falling on the QD. The probe field induces an electric dipole in each QE in the ensemble. Therefore, QEs are interacting with each other via the DDI coupling and produce the DDI electric field. This field is denoted as the DDI-QE field ( $\mathbf{E}_{\text{DDI}}^{\text{QE}}$ ). Similarly, the probe field also induces an electric dipole in each QD in the ensemble. Hence, QDs interact with each other via DDI and produce the DDI field which is denoted as the DDI-QD field ( $\mathbf{E}_{\text{DDI}}^{\text{QD}}$ ). Both DDI fields are calculated using the DDI theory of Refs. [26–28].

When the probe field  $\mathbf{E}_P$  falls on a QE, it induces a polarization  $\mathbf{P}_{\text{QE}}$ , which in turn produces a dipole electric field

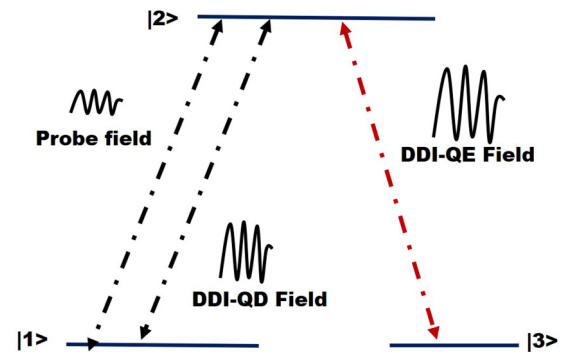


FIG. 2. A schematic diagram of a three-level QD is plotted. Energy levels are denoted as  $|1\rangle$ ,  $|2\rangle$ , and  $|3\rangle$ . The probe field and DDI-QD field are applied in the transition  $|1\rangle \leftrightarrow |2\rangle$ . The DDI-QE field is acting in the transitions  $|2\rangle \leftrightarrow |3\rangle$ .

$\mathbf{E}_{\text{QE}}$ . The expression of the electric field is derived in Ref. [26] and it is written as

$$\mathbf{E}_{\text{QE}} = \frac{\mathbf{P}_{\text{QE}}}{4\pi\epsilon_b r_s^3}, \quad (12)$$

where the expression for  $\mathbf{P}_{\text{QE}}$  is found as

$$P_{\text{QE}} = 4\pi\epsilon_b R_{\text{QE}}^3 g_l \zeta_{\text{QE}} E_P, \quad \zeta_{\text{QE}} = \frac{\epsilon_q - \epsilon_c}{\epsilon_q + 2\epsilon_c}, \quad (13)$$

where the constant  $g_l$  is called the polarization parameter and it has values  $g_l = 2$  and  $-1$  for  $\mathbf{P}_{\text{QE}} \parallel \mathbf{E}_P$  and  $\mathbf{P}_{\text{QE}} \perp \mathbf{E}_P$  [27,28]. The expression of  $\epsilon_c$  is given by Eq. (2). The constant  $R_{\text{QE}}$  is the radius of the QE and  $r_s$  is the distance between the center of the QD and the QE.

In the rest of the paper, we have taken  $\mathbf{P}_{\text{QE}} \parallel \mathbf{E}_P$ . This means that we will take  $g_l = +2$  in our numerical calculations. Note that we have not used the vector notation for the  $P_{\text{QE}}$  and  $E_P$  in Eq. (13). The reason is that  $P_{\text{QE}}$  and  $E_P$  are either parallel or perpendicular to each other. The polarization  $g_l$  controls the direction between  $P_{\text{QE}}$  and  $E_P$ . The  $g_l$  notation has been used widely in plasmonic research [13–19].

The DDI electric field due to the ensemble of QEs is calculated in Ref. [26] and found as follows:

$$\mathbf{E}_{\text{DDI}}^{\text{QE}} = \frac{\lambda_d}{3} \frac{\mathbf{P}_{\text{QE}}}{4\pi\epsilon_b r_s^3}. \quad (14)$$

The constant  $\lambda_d$  is called the DDI constant. Putting the expression of  $P_{\text{QE}}$  from Eq. (13) into the above Eq. (14) we get

$$\mathbf{E}_{\text{DDI}}^{\text{QE}} = \Lambda_{\text{DDI}}^{\text{QE}} \mathbf{E}_P, \quad \Lambda_{\text{DDI}}^{\text{QE}} = \frac{\lambda_d R_{\text{QE}}^3 g_l}{3r_s^3} \left( \frac{\epsilon_{\text{QE}} - \epsilon_c}{\epsilon_{\text{QE}} + 2\epsilon_c} \right), \quad (15)$$

where  $\Lambda_{\text{DDI}}^{\text{QE}}$  is called the DDI-QE coupling constant.

Similarly, we can calculate the DDI electric field produced by QDs as follows:

$$\mathbf{E}_{\text{DDI}}^{\text{QD}} = \Lambda_{\text{DDI}}^{\text{QD}} \mathbf{E}_P, \quad \Lambda_{\text{DDI}}^{\text{QD}} = \frac{\lambda_d R_{\text{QD}}^3 g_l}{3r_s^3} \left( \frac{\epsilon_{\text{QD}} - \epsilon_c}{\epsilon_{\text{QD}} + 2\epsilon_c} \right), \quad (16)$$

where  $R_{\text{QD}}$  is the radius of the QD. Here  $\Lambda_{\text{DDI}}^{\text{QD}}$  is called the DDI-QD coupling constant.

Now, we calculate the exciton decay linewidths (rates). We consider that the probe electric field  $E_P$  with energy  $\epsilon_{nm,z}$  is acting between transition  $|1\rangle \leftrightarrow |2\rangle$ . The PL emission occurs when an exciton falls from the excited state  $|2\rangle$  to the ground state  $|1\rangle$ . Next, we consider the DDI-QD field  $E_{\text{DDI}}^{\text{QD}}$  is also acting between transition  $|2\rangle \leftrightarrow |1\rangle$ . We apply the DDI-QE field  $E_{\text{DDI}}^{\text{QE}}$  between transition  $|2\rangle \leftrightarrow |3\rangle$ . See the schematic diagram of the QD in Fig. 2.

We calculate two exciton spontaneous decay linewidths. The first is due to the spontaneous decay of the exciton from the excited state  $|2\rangle$  to the ground state  $|1\rangle$  and it is called the SP linewidth ( $\Gamma_{\text{SP}}$ ). The exciton coupling with the probe and DDI-QD fields is responsible for this decay linewidth. On the other hand, the second linewidth is due to the spontaneous decay of the exciton from the excited state  $|2\rangle$  to the ground state  $|3\rangle$ . This decay linewidth is due to the exciton coupling with the DDI-QE field and it is called the DDI-QE linewidth

( $\Gamma_{\text{DDI}}^{\text{QE}}$ ). The exciton interaction Hamiltonian is written as

$$H = H_0 + H_{\text{SP}} + H_{\text{DDI}}^{\text{QE}}, \quad (17)$$

where

$$H_0 = \sum_{i=1,3} \epsilon_{2i} \sigma_{2i} + \sum_{nm} \sum_{k_z} \epsilon_{nm,k_z} p_{nm,k_z}^\dagger p_{nm,k_z}, \quad (18)$$

$$H_{\text{SP}} = \sum_{nm} \sum_{k_z} V_{\text{SP}} (p_{nm,k_z} \sigma_{21}^\dagger + p_{nm,k_z}^\dagger \sigma_{21}), \quad (19)$$

$$H_{\text{DDI}}^{\text{QE}} = \sum_{nm} \sum_{k_z} V_{\text{DDI}}^{\text{QE}} (p_{nm,k_z} \sigma_{23}^\dagger + p_{nm,k_z}^\dagger \sigma_{23}), \quad (20)$$

where the operators  $p_{nm,k_z}^\dagger$  and  $p_{nm,k_z}$  are the photon creation and annihilation operators, respectively. Here  $\sigma_{2i} = |2\rangle\langle i|$  is the exciton creation operator for transition  $|2\rangle \leftrightarrow |i\rangle$  where  $i = 1, 3$ . Other physical coupling parameters are found as

$$V_{\text{SP}}(\epsilon_{nm,k_z}) = i \left( \frac{\mu_{21}^2 \epsilon_{nm,k_z}}{2\epsilon_0 \epsilon_b V_{\text{QD}}} \right)^{1/2} (1 + \Lambda_{\text{DDI}}^{\text{QD}})^{1/2}, \quad (21)$$

$$V_{\text{DDI}}^{\text{QE}}(\epsilon_{nm,k_z}) = i \left( \frac{\mu_{23}^2 \epsilon_{nm,k_z}}{2\epsilon_0 \epsilon_b V_{\text{QD}}} \right)^{1/2} (\Lambda_{\text{DDI}}^{\text{QE}})^{1/2}, \quad (22)$$

where  $V_{\text{QD}}$  is the volume of the QD. Here  $H_0$  is the noninteracting Hamiltonian of the QD and the bound photons in the nanofiber. The second term  $H_{\text{SP}}$  is the interaction between the exciton with the probe and DDI-QD fields. This term is responsible for the decay of the exciton from  $|2\rangle$  to  $|1\rangle$ . The last term  $H_{\text{DDI}}^{\text{QE}}$  is the interaction between the exciton with the DDI-QE field and it is responsible for the decay of the exciton from  $|2\rangle$  to  $|3\rangle$ .

The SP linewidth and the DDI-QE linewidth are evaluated by using Fermi's "golden rule" method of the quantum-mechanical perturbation theory. It is written as follows:

$$\Gamma_{ij} = 2\pi \sum_{nm} \sum_{k_z} |V_{\text{int}}(\epsilon_k)|^2 \delta(\epsilon_{nm,k_z} - \epsilon_{ij}) \quad (23)$$

where  $V_{\text{int}}$  is the interaction coupling term given in Eqs. (21) and (22). Let us replace the summation over  $k_z$  by the integration by using the method of the DOS. It is written as

$$\sum_{k_z} = \int D_{nm}(\epsilon_{nm,k_z}) d\epsilon_{nm,k_z} \quad (24)$$

where  $D_{nm}$  is the DOS of the bound photons inside the NFH and is written as

$$D_{nm}(\epsilon_{nm,k_z}) = \frac{L}{\pi} \left( \frac{dk_z}{d\epsilon_{nm,k_z}} \right), \quad (25)$$

where  $L$  is the length of the nanofiber. Inserting Eq. (25) into Eq. (23) we get the expression of the decay linewidth in terms of the DOS as follows:

$$\Gamma_{ij} = 2\pi \sum_{nm} \int d\epsilon_{nm,k_z} D_{nm}(\epsilon_{nm,k_z}) |V_{\text{int}}(\epsilon_{nm,k_z})|^2 \delta(\epsilon_{nm,k_z} - \epsilon_{ij}). \quad (26)$$

Let us evaluate the DOS appearing in Eq. (25). With the help of Eq. (11), we evaluated the DOS and found the follow-

ing expression:

$$D_{nm}(\varepsilon_{nm,k_z}) = \frac{V_{\text{NF}} \varepsilon_{nm,k_z}^2}{\pi^2 \hbar^3 c^3} \left( \frac{G_c(\varepsilon_{nm,k_z}) F_c(\varepsilon_{nm,k_z})}{[F_c^2(\varepsilon_{nm,k_z}) - F_c^2(\varepsilon_{nm})]^{1/2}} \right), \quad (27)$$

where

$$G_c(\varepsilon_{nm,k_z}) = \frac{\hbar^2 c^2}{A \varepsilon_{nm,k_z}^2 \sqrt{\varepsilon_c}}. \quad (28)$$

Here  $V_{\text{NF}}$  and  $A$  are the volume and cross-sectional area of the nanofiber, respectively. Note that the DOS depends on the function  $F_c$  which in turn depends on the dielectric constant of the core material. When the  $\varepsilon_{nm,k_z}$  is close to  $\varepsilon_{nm}$ , the denominator in Eq. (27) becomes small and the DOS becomes large.

Let us calculate the SP linewidth ( $\Gamma_{\text{SP}}$ ) using Eq. (26). Putting Eqs. (27) and (21) into Eq. (23) and doing extensive mathematical manipulations, we get the linewidth for the exciton from  $|2\rangle$  to  $|1\rangle$  as

$$\Gamma_{\text{SP}} = \gamma_0 |1 + \Lambda_{\text{DDI}}^{\text{QD}}(\varepsilon_{21})| \sum_{nm} \left\{ \frac{G_c(\varepsilon_{21}) F_c(\varepsilon_{21})}{[F_c^2(\varepsilon_{21}) - F_c^2(\varepsilon_{nm})]^{1/2}} \right\}, \quad (29)$$

where

$$\gamma_0 = \left( \frac{\hbar \mu_{21}^2 \varepsilon_{21}^3}{\pi \varepsilon_0 \varepsilon_b \hbar^4 c^3} \right). \quad (30)$$

Here  $\gamma_0$  is the spontaneous decay linewidth when the QD is in the vacuum.

Similarly, we calculate the DDI-QE linewidth ( $\Gamma_{\text{DDI}}^{\text{QE}}$ ) for the exciton decaying from  $|2\rangle$  to  $|3\rangle$ . Inserting Eqs. (27) and (22) into Eq. (23) and doing extensive mathematical manipulations, we found an analytical expression of the linewidth as

$$\Gamma_{\text{DDI}}^{\text{QE}} = \gamma_0 |\Lambda_{\text{DDI}}^{\text{QE}}(\varepsilon_{23})| \sum_{nm} \left\{ \frac{G_c(\varepsilon_{23}) F_c(\varepsilon_{23})}{[F_c^2(\varepsilon_{23}) - F_c^2(\varepsilon_{nm})]^{1/2}} \right\}. \quad (31)$$

It is interesting to note that both linewidths depend on physical parameters of the nanofiber such as the size and shape of the nanofiber along with the concentration of QDs and QEs and their dielectric constants. See the expression of  $F_c$  in Eq. (4).

We found that both SP and DDI-QE linewidths ( $\Gamma_{\text{SP}}$ ,  $\Gamma_{\text{DDI}}^{\text{QE}}$ ) are enhanced when exciton energies  $\varepsilon_{21}$  and  $\varepsilon_{23}$  lie near the  $\varepsilon_{nm}$ . This is because the denominators in Eqs. (26) and (28) become small. We also predicted that the linewidths are also enhanced due to the DDI-QD and DDI-QE coupling constants.

Furthermore, we also found that the linewidths are quenched or depressed when exciton energies  $\varepsilon_{21}$  and  $\varepsilon_{23}$  lie far away from the exciton energy  $\varepsilon_{nm}$ . In this case, the denominator of Eqs. (29) and (31) becomes large and hence linewidths become small (quenched). The quenching occurs when DDI-QE and DDI-QD coupling constants are weak.

#### IV. PHOTOLUMINESCENT AND DENSITY-MATRIX METHOD

In this section, we calculate the photoluminescence using the density-matrix method. The PL emission occurs when an exciton falls from the excited state  $|2\rangle$  to the ground state  $|1\rangle$ . In Fig. 2, two electric fields are acting between these two states, namely,  $E_P$  and  $E_{\text{DDI}}^{\text{QD}}$ . These two fields induce a polarization  $\mathbf{P}_{\text{QD}}$  in the QD and it is written as

$$\mathbf{P}_{\text{QD}}(\varepsilon_{nm,k_z}) = \varepsilon_0 \varepsilon_c \chi_{\text{QD}}(\varepsilon_{nm,k_z}) (\mathbf{E}_P + \mathbf{E}_{\text{DDI}}^{\text{QD}}), \quad (32)$$

where  $\chi_{\text{QD}}$  is the susceptibility of the QD.

It is important to note that in Eq. (32), the electric fields  $E_P$  and  $E_{\text{DDI}}^{\text{QD}}$  are parallel to each other (i.e.,  $E_{\text{DDI}}^{\text{QD}} \parallel E_P$ ). For example, see Eq. (15). In this paper, we have taken  $\mathbf{P}_{\text{QD}} \parallel E_P$ . For example, see Eq. (6). Therefore, one can easily take out the vector notation from Eq. (32).

We can express the polarization of the QD in terms of the quantum density-matrix operator ( $\rho$ ) as follows [29,30]:

$$P_{\text{QD}}(\varepsilon_{nm,k_z}) = \frac{2\mu_{21}\rho_{21}(\varepsilon_{nm,k_z})}{V_{\text{QD}}}, \quad (33)$$

where  $\mu_{21}$  is the matrix elements of the dipole moment between transition  $|1\rangle \leftrightarrow |2\rangle$  and  $\rho_{21}$  is the density-matrix operator ( $\rho$ ) between transition  $|1\rangle \leftrightarrow |2\rangle$ .

Note that in Eq. (33), we have not used the vector notation for the  $P_{\text{QE}}$  and  $\mu_{21}$  since they are parallel to each other. This notation has been used widely in plasmonic research [13–19].

By comparing Eqs. (32) and (33), we found the relationship between the susceptibility and the density-matrix element as follows:

$$\chi_{\text{QD}}(\varepsilon_{nm,k_z}) = \frac{2\mu_{21}\rho_{21}(\varepsilon_{nm,k_z})}{\varepsilon_0 \varepsilon_c V_{\text{QD}} (E_P + E_{\text{DDI}}^{\text{QD}})}. \quad (34)$$

The intensity of the photoluminescence from the QD can be calculated in terms of the susceptibility as follows:

$$I_{\text{PL}} = \frac{\varepsilon_{nm,k_z} V_{\text{QD}}}{2\hbar} \text{Im} \{ \varepsilon_0 \chi_{\text{QD}}(\varepsilon_{nm,k_z}) \} |E_P + E_{\text{DDI}}^{\text{QD}}|^2, \quad (35)$$

where  $E_P$  and  $E_{\text{DDI}}^{\text{QD}}$  are acting in the transition  $|1\rangle \leftrightarrow |2\rangle$ . Substituting Eq. (34) into Eq. (35), we get the expression of PL in terms of the density matrix as

$$I_{\text{PL}} = \left( \frac{\mu_{21} \varepsilon_{nm,k_z}}{2\hbar \varepsilon_c} \right) \text{Im} [\rho_{21}(\varepsilon_{nm,k_z})] |E_P + E_{\text{DDI}}^{\text{QD}}|. \quad (36)$$

The photoluminescence depends on the density-matrix elements  $\rho_{21}$ . The PL has two contributions: the first is due to the emission of probe field photons and the second contribution is the surface plasmon polariton (SPP) field photons. This means we found that the PL intensity is enhanced due to the SPP field.

We have shown in Fig. 2 that the probe field  $E_P$  and the DDI-QD field  $E_{\text{DDI}}^{\text{QD}}$  are acting between transition  $|2\rangle \leftrightarrow |1\rangle$ . The DDI-QE field  $E_{\text{DDI}}^{\text{QE}}$  is acting between transition  $|2\rangle \leftrightarrow |3\rangle$ . Using the dipole and rotating wave approximation [29,30], the interaction Hamiltonian is found as follows:

$$H_{\text{int}} = \Omega_P \sigma_{21} + \Omega_P \Lambda_{\text{DDI}}^{\text{QD}} \sigma_{21} + \Omega_P \Lambda_{\text{DDI}}^{\text{QE}} \sigma_{23} + \text{H.c.} \quad (37)$$

Here  $\Omega_p = \mu_{21}E_p$  is the Rabi energy and H.c. stands for the Hermitian conjugate. The first term in the Hamiltonian is the exciton-probe field interaction due to the transitions  $|2\rangle \leftrightarrow |1\rangle$ . The second term is the exciton interaction with the DDI-QD field due to transitions  $|2\rangle \leftrightarrow |1\rangle$ . The third term is the exciton interaction with the DDI-QE field due to transitions  $|2\rangle \leftrightarrow |3\rangle$ .

Now we evaluate an analytical expression of the density-matrix element  $\rho_{21}$ . With the help of Eq. (37), we solve the density-matrix equations [29,30] in the steady state. We consider that the electron population of the ground state  $|1\rangle$  is larger than the excited states  $|2\rangle$  and  $|3\rangle$ . After extensive mathematical manipulations, we find the following analytical expression of the density-matrix element

$\rho_{21}$ :

$$\rho_{21} = \frac{-i(\Omega_p + \Omega_p \Lambda_{\text{DDI}}^{\text{QD}})[\delta_{31} + i(\Gamma_{\text{SP}} + \Gamma_{\text{DDI}}^{\text{QE}})/2]}{(\delta_{21} + i\Gamma_{\text{SP}})[\delta_{31} + i(\Gamma_{\text{SP}} + \Gamma_{\text{DDI}}^{\text{QE}})/2] + (\Omega_p \Lambda_{\text{DDI}}^{\text{QE}})^2}, \quad (38)$$

where  $\delta_{21}$  is called the probe detuning and is found as

$$\begin{aligned} \delta_{21} &= \varepsilon_{nm,k_z} - \varepsilon_{21}, \\ \delta_{23} &= \varepsilon_{nm,k_z} - \varepsilon_{23}, \\ \delta_{31} &= \delta_{21} - \delta_{23}. \end{aligned} \quad (39)$$

Finally, we get the analytical expression of the PL by combining Eqs. (38) and (36) as

$$I_{\text{PL}} = I_0 \text{Im} \left( \frac{-i[\delta_{31} + i(\Gamma_{\text{SP}} + \Gamma_{\text{DDI}}^{\text{QE}})/2]}{(\delta_{21} + i\Gamma_{\text{SP}})[\delta_{31} + i(\Gamma_{\text{SP}} + \Gamma_{\text{DDI}}^{\text{QE}})/2] + (\Omega_p \Lambda_{\text{DDI}}^{\text{QE}})^2} \right) |\Omega_p + \Omega_p \Lambda_{\text{DDI}}^{\text{QD}}|^2, \quad (40)$$

where

$$I_0 = \frac{\varepsilon_{21} \Omega_p}{2\hbar \varepsilon_c}. \quad (41)$$

We found that the analytical expression of the PL depends on the radiative decay linewidths  $\Gamma_{\text{SP}}$  and  $\Gamma_{\text{DDI}}^{\text{QE}}$  which in turn depend on the SPP and DDI couplings along with the physical parameters of the nanofiber.

From the PL expression in Eq. (40), we predict that the PL is enhanced due to SPP coupling since it appears in the numerator. We also show that the PL is quenched due to the DDI-QE coupling which is located in the denominator.

## V. RESULTS AND DISCUSSIONS

In this section, we perform numerical simulation for the SP linewidth, DDI-QE linewidth, and PL intensity. We also compare our theory of the photoluminescence with experiments of Ref. [12]. In this reference, authors have fabricated a core-shell nanofiber where the core is fabricated from P4VP material and the shell is made from PS material. They have embedded an ensemble of the CdSe QDs and S101 dye molecules in the core. They measured the photoluminescence intensity of the CdSe QD by varying the number of dye molecules.

The experimental physical parameters for the numerical simulations are taken as follows. The average radius of the CdSe QDs and S101 molecule is found as  $R_{\text{QD}} = 1.5$  nm,  $r_s = 5.3$  nm, and  $R_{\text{QE}} = 0.6$  nm, respectively [12,23]. The emission spectrum of CdSe QDs is centered at  $\lambda_{12} = 541$  nm which is converted to energy units as  $\varepsilon_{21} = 2.3$  eV [12]. The dielectric constant of the core material P4VP is found as  $\varepsilon_b = 3.8$  and the dielectric constant of the shell material PS is taken as  $\varepsilon_s = 2.6$ . Other parameters are taken as  $\varepsilon_{\text{QE}} = 3.1$  [22],  $\varepsilon_{\text{QD}} = 5.9$  [21],  $g_l = 2$ ,  $\gamma_d = 1$ , and the radius of nanofiber is taken as 400 nm.

Let us first calculate the number of bound states located in the core-shell nanofiber where the core is fabricated from

P4VP and the shell is made from PS. We use Eq. (8) to calculate the value of  $k_x$  and  $k_y$  for a given quantum number  $n$  and  $m$ . We have plotted  $F_x$  as a function  $k_x$  in Fig. 3. The solid, dashed, and dash-dotted curves are plotted for  $n = 0, 1, 2$ , respectively. Note that the solid curve becomes zero at  $k_x = 1.96 \times 10^6 \text{ m}^{-1}$ . This is the quantized value of  $k_x = k_n$  for  $n = 0$ . The dashed and dash-dotted curves become zero at  $k_x = k_n = 5.89 \times 10^6 \text{ m}^{-1}$  and  $k_x = k_n = 9.81 \times 10^6 \text{ m}^{-1}$  for  $n = 1$  and  $2$ , respectively. Similarly, we can also find the quantized values of  $k_y$  for  $m = 0, 1, 2$ . They are found as  $k_y = k_m = 1.96 \times 10^6, 5.89 \times 10^6$ , and  $9.81 \times 10^6 \text{ m}^{-1}$  for  $m = 0, 1, 2$ , respectively.

With the help of the quantized value of  $k_n$  and  $k_m$  along with Eq. (9), we can calculate the quantized energy  $\varepsilon_{nm}$  as  $\varepsilon_{00} = 1.23$  eV,  $\varepsilon_{01} = \varepsilon_{10} = 2.76$  eV, and  $\varepsilon_{11} = 3.7$  eV. Here we have considered the depth of the photonic quantum well is equal to 2.3 eV which is the exciton energy of the CdSe QD.

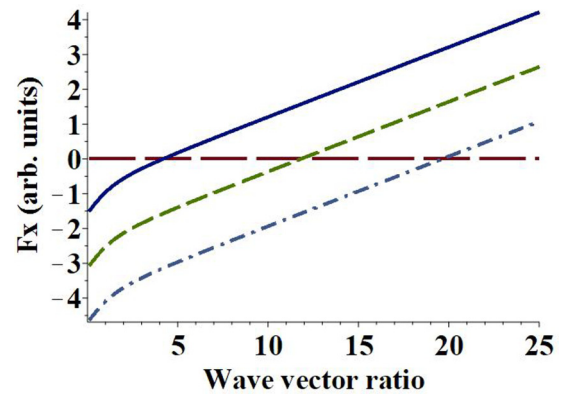


FIG. 3. The function  $F_x$  appearing in Eq. (8) is plotted as a function of the wave-vector ratio ( $k_x/k_0$ ) where  $k_0 = 10^{-6} \text{ m}^{-1}$ . The solid, dashed, and dash-dotted curves are plotted for  $n = 0, 1, 2$ , respectively. Note that all three curves changes from negative to positive values. The crossing points are located at  $k_x/k_0 = 1.96, 5.89$ , and  $9.81$  for  $n = 0, 1$ , and  $2$ , respectively.

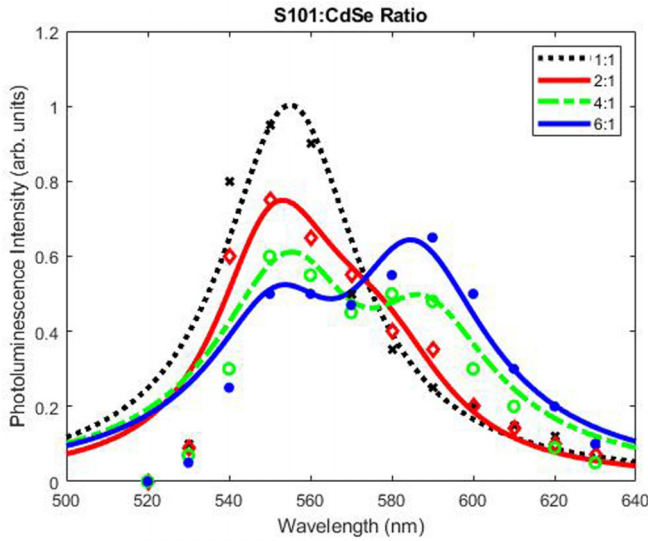


FIG. 4. The theoretical and experiential results for PL intensity (arb. units) are plotted as a function of wavelength (nm). The crosses, open diamonds, open circles, and solid circles correspond to the ratio of S101: CdSe in amounts 1:1, 2:1, 4:1, and 6:1. The dotted, red solid, green dotted, and blue solid theoretical curves correspond to samples 1:1, 2:1, 4:1, and 6:1 respectively.

According to quantum mechanics, the energy of the bound photon state must not be larger than the depth of the quantum well. Hence, from the above calculations, we have only one bound state, which is  $\varepsilon_{00} = 1.23$  eV.

Now, we compare our theory with experiential results of Ref. [12]. The theoretical and experiential results for PL intensity are plotted in Fig. 4 as a function of wavelength for the different ratios of CdSe QDs ( $n_{\text{QD}}$ ) and S101 dye ( $n_{\text{QE}}$ ). The ratio is denoted as  $[n_{\text{QD}}: n_{\text{MNP}}]$ . The crosses, open diamonds, open circles, and solid circles correspond to the ratio of S101: CdSe in amounts 1:1, 2:1, 4:1, 6:1.  $[n_{\text{QD}}: n_{\text{MNP}}]$  of CdSe QDs and S101 dye samples as [1: 0], [1: 0.1], [1: 0.3], and [1: 0.5], respectively. The theoretical PL curves are overlaid on top of the experiential data. The dotted, dashed, dash-dotted, and solid theoretical curves correspond to the concentration ratio  $[n_{\text{QD}}: n_{\text{QE}}]$  as [1: 0], [1: 0.1], [1: 0.3], and [1: 0.5], respectively. The curve [1: 0] is for CdSe QDs alone.

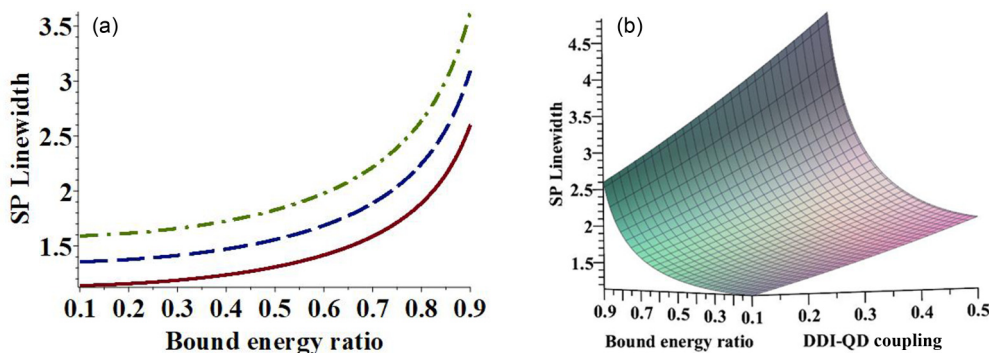


FIG. 5. (a) The SP linewidth ( $\Gamma_{\text{SP}}/\gamma_0$ ) is plotted as a function of the bound energy ratio  $|\varepsilon_{21}/\varepsilon_{nm}|$  where  $\varepsilon_{nm}$  is the bound photon state energy and  $\varepsilon_{21}$  is the exciton energy. The solid, dashed, and dash-dotted lines correspond to the DDI-QD coupling  $\Lambda_{\text{DDI}}^{\text{QD}} = 0.1, 0.2,$  and  $0.3,$  respectively. (b) The decay linewidth  $\Gamma_{\text{SP}}/\gamma_0$  is plotted as a function of the bound energy ratio  $|\varepsilon_{21}/\varepsilon_{nm}|$  and the DDI-QD coupling ( $\Lambda_{\text{DDI}}^{\text{QD}}$ ).

Note that a good agreement between our theory and experiment is found. We plotted the theoretical curves using the following parameters:  $\Gamma_{\text{SP}} = 0.2,$   $\Gamma_{\text{DDI}}^{\text{QE}} = 0.3,$   $\Omega_P/\gamma_0 = 0.2,$  and the parameter  $\Lambda_{\text{DDI}}^{\text{QE}}$  varied according to concentration as 0.1, 0.3, 0.6, and 1.1, for the ratios of 1:1, 1:2, 1:4, and 1:6, respectively. The parameters for the QDs are stated previously and are the same.

Note that as the concentration of the S101 dye molecules is increased the one peak of the PL spectrum splits into two peaks. The physics of splitting can be explained as follows. In our theory, we have considered that PL emission is due to the transition  $|2\rangle \leftrightarrow |1\rangle$ . Therefore, the single peak in the PL spectrum is due to the transition  $|2\rangle \leftrightarrow |1\rangle$ . Remember that the DDI-QE field is due to an ensemble of dye molecules and it acts between the transition  $|2\rangle \leftrightarrow |3\rangle$ . When the concentration of dye molecules increases, the DDI-QE coupling constant also increases and reaches the strong-coupling limit. Therefore, when the DDI-QE coupling is in the strong-coupling limit, two dressed states are created in the system. The transition  $|2\rangle \leftrightarrow |1\rangle$  splits into two dressed states called  $|2_{-}\rangle \leftrightarrow |1\rangle$  and  $|2_{+}\rangle \leftrightarrow |1\rangle$ . Therefore, the PL transition occurs due to transitions  $|2_{-}\rangle \leftrightarrow |1\rangle$  and  $|2_{+}\rangle \leftrightarrow |1\rangle$  and the PL spectrum has two peaks. That is why one peak in the PL spectrum splits into two peaks.

Next, we perform numerical simulations of the SP linewidth ( $\Gamma_{\text{SP}}$ ), DDI-QE linewidth ( $\Gamma_{\text{DDI}}^{\text{QE}}$ ), and PL for a general NFH. In our calculations, all energies such as Rabi frequency, exciton frequencies, probe detuning, and decay linewidth are measured with respect to the decay linewidth  $\gamma_0$ . We have considered that the Rabi frequency is  $\Omega_P/\gamma_0 = 1$  and the DDI-QE field energy is in resonance with the exciton energy  $\varepsilon_{22}$  (i.e.,  $\delta_{21} = 0$ ).

We have shown that the PL spectrum depends on the decay SP linewidths ( $\Gamma_{\text{SP}}$ ) and ( $\Gamma_{\text{DDI}}^{\text{QE}}$ ). We found that these decay linewidths play an important role in the splitting of the PL peak. Let us first study the effect of the bound photon states  $\varepsilon_{nm}$  on the decay linewidth of  $\Gamma_{\text{SP}}$ . We have plotted the normalized decay linewidth ( $\Gamma_{\text{SP}}/\gamma_0$ ) as a function of the energy ratio ( $|\varepsilon_{21}/\varepsilon_{nm}|$ ). The results are plotted in Fig. 5(a). We have taken  $L = 400$  nm and  $\varepsilon_{21} = 2.3$  eV. The solid, dashed, and dash-dotted lines correspond to the DDI-QD coupling  $\Lambda_{\text{DDI}}^{\text{QD}} = 0.1, 0.2,$  and  $0.3,$  respectively. One can see that as the energy ratio  $|\varepsilon_{21}/\varepsilon_{nm}|$  lies close to  $|\varepsilon_{21}/\varepsilon_{nm}| = 1,$

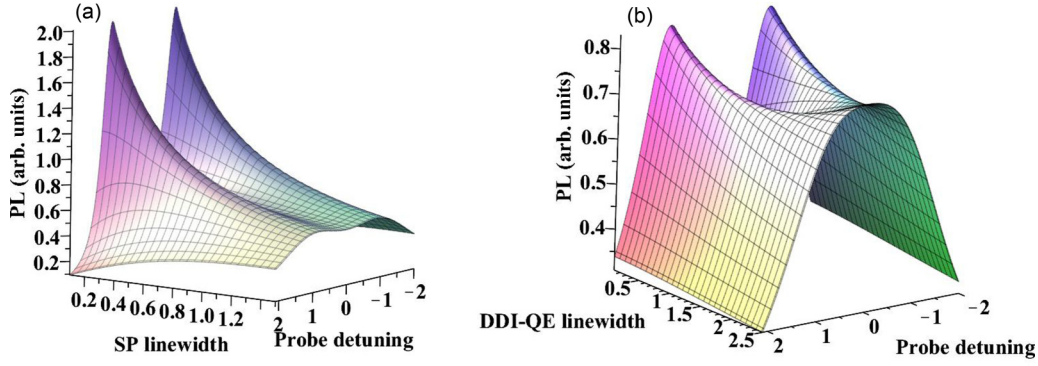


FIG. 6. (a) The PL (arb. units) is plotted as a function of the probe detuning ( $\delta_{21}/\gamma_0$ ) and the radiative linewidth ( $\Gamma_{\text{DDI}}^{\text{QE}}/\gamma_0$ ). (b) The PL is plotted as a function of the probe detuning ( $\delta_{21}/\gamma_0$ ) and the decay linewidth ( $\Gamma_{\text{DDI}}^{\text{QE}}/\gamma_0$ ).

there is the enhancement in decay linewidth. On the other hand, when the energy ratio  $|\varepsilon_{21}/\varepsilon_{nm}|$  lies far away from the  $|\varepsilon_{21}/\varepsilon_{nm}| = 1$ , there is the suppression of the decay linewidth.

The enhancement in the spontaneous decay linewidths is explained as follows. The decay linewidth is inversely proportional to  $(\varepsilon_{nm} - \varepsilon_{21})$  as shown in Eq. (26). When the bound photon energy  $\varepsilon_{nm}$  lies close to the exciton energy  $\varepsilon_{21}$  the denominator becomes small. That is why the decay linewidth is enhanced when the bound photon energy is close to the exciton energy. Note that the decay linewidth is also enhanced due to the DDI-QD coupling. This is because that the linewidth is proportional to the DDI-QD coupling  $\Lambda_{\text{DDI}}^{\text{QD}}$  [see Eq. (26)].

To make the enhancement of the decay linewidth clearer, we have also plotted the SP linewidth as a function of  $|\varepsilon_{21}/\varepsilon_{nm}|$ . The decay linewidth ( $\Gamma_{\text{PS}}/\gamma_0$ ) is plotted as a function of the energy ratio ( $|\varepsilon_{21}/\varepsilon_{nm}|$ ) and the DDI-QD coupling ( $\Lambda_{\text{DDI}}^{\text{QD}}$ ). The results are plotted in Fig. 5(b). Note that the decay linewidth is enhanced when the bound photon energy is close to the exciton energy. There is also enhancement due to the presence of the DDI-QD coupling. The decay linewidth is depressed when the bound photon energy is far away from the exciton energy and the DDI-QD coupling is weak. Similar results are also found for the decay linewidth  $\Gamma_{\text{DDI}}^{\text{QE}}$ . We conclude that the value of the decay linewidth can be controlled by the properties of the nanofiber and doping of the QDs and QEs.

Note that in Figs. 5(a) and 5(b), we have plotted the SP linewidth as a function of  $|\varepsilon_{21}/\varepsilon_{nm}|$  rather than  $|\varepsilon_{nm} - \varepsilon_{21}|$ . The reason is that we wanted to plot the SP linewidth for a general nanofiber. One can also plot the SP linewidth as a function of  $|\varepsilon_{nm} - \varepsilon_{21}|$  and can get similar figures and the same physics. This is because one can express  $|\varepsilon_{nm} - \varepsilon_{21}| = \varepsilon_{nm}|1 - \varepsilon_{21}/\varepsilon_{nm}|$  where  $\varepsilon_{nm}$  is absorbed in the normalization. One can see that for the first case when  $|\varepsilon_{21}/\varepsilon_{nm}| = 1$  the SP linewidth has a maximum value. Similarly, in the second case, when  $\varepsilon_{nm} = \varepsilon_{21}$  the SP linewidth has also a maximum value. It is noted that in the second case, the  $|\varepsilon_{nm} - \varepsilon_{21}|$  axis has a unit of energy (eV) and the figures are valid for a particular plasmonic nanofiber. On the other hand, in the first case, the  $|\varepsilon_{21}/\varepsilon_{nm}|$  axis is unitless and the figures are valid for all types of the plasmonic nanofiber.

Finally, we study the effect of decay linewidths  $\Gamma_{\text{SP}}$  and  $\Gamma_{\text{DDI}}^{\text{QE}}$  on the PL spectrum. First, we have studied the effect of decay linewidths  $\Gamma_{\text{SP}}$  on the PL spectrum in Fig. 6(a).

The PL (arb. units) is plotted as a function of the probe detuning ( $\delta_{21}/\gamma_0$ ) and the decay linewidth ( $\Gamma_{\text{DDI}}^{\text{QE}}/\gamma_0$ ). Note that  $\Gamma_{\text{SP}}$  changes with the DDI-QD coupling constant which in turn changes with the distance between the QDs and QEs. This also changes with the location of bound-state energies as shown in Fig. 5. The value of the DDI-QE is taken in the strong-coupling limit ( $\Lambda_{\text{DDI}}^{\text{QE}} = 1.5$ ) so that we can get splitting in the PL spectrum. Other physical parameters are taken as  $\Lambda_{\text{DDI}}^{\text{QD}} = 0.1$  and  $(\Gamma_{\text{DDI}}^{\text{QE}}/\gamma_0) = 1$ . It is interesting to note that at low values of the decay linewidth ( $\Gamma_{\text{SP}}/\gamma_0$ ) the PL spectrum has two peaks. As the strength of the decay linewidth increases the two peaks merge into one peak. At the same time, the intensity of the PL spectrum decreases. The height of the PL spectrum decreases because the intensity of the peak is inversely proportional to the decay linewidth (Eq. (40)). The physics of the merging of peaks will be explained along with Fig. 6(b).

In Fig. 6(b), we study the effect of the DDI-QE linewidth  $\Gamma_{\text{DDI}}^{\text{QE}}$  on the PL spectrum. The PL is plotted as a function of the probe detuning ( $\delta_{21}/\gamma_0$ ) and the decay linewidth ( $\Gamma_{\text{DDI}}^{\text{QE}}/\gamma_0$ ). Note  $\Gamma_{\text{DDI}}^{\text{QE}}$  changes with the DDI-QE coupling constant which in turn changes with the distance between the QEs and QDs. This also changes with the location of bound-state energies. The value of the DDI-QE is taken in the strong-coupling limit ( $\Lambda_{\text{DDI}}^{\text{QE}} = 1.5$ ). Other physical parameters are taken as  $\Lambda_{\text{DDI}}^{\text{QD}} = 0.1$  and  $\Gamma_{\text{SP}}/\gamma_0 = 1$ . We found that when the decay linewidth ( $\Gamma_{\text{DDI}}^{\text{QE}}/\gamma_0$ ) is weak, the PL spectrum has two peaks. As the strength of the decay linewidth increases the two peaks merge into one peak. In this case, the intensity of the PL spectrum does not change. The intensity of the PL spectrum does not change because the decay linewidth  $\Gamma_{\text{DDI}}^{\text{QE}}$  appears in both the numerator and denominator of the PL expression. For example, see Eq. (37). Hence, they cancel each other and there is no change in the intensity of the PL spectrum.

The physics of the merging of two peaks into one peak in Figs. 6(a) and 6(b) can be explained as follows. Two peaks in the PL spectrum are due to transitions  $|2_{-}\rangle \leftrightarrow |1\rangle$  and  $|2_{+}\rangle \leftrightarrow |1\rangle$ . We know that the distance between two peaks is approximately equal to the energy difference between  $|2_{+}\rangle$  and  $|2_{-}\rangle$ , i.e.,  $(\varepsilon_{2_{+}} - \varepsilon_{2_{-}})$ . The decay linewidths ( $\Gamma_{\text{SP}}$  and  $\Gamma_{\text{DDI}}^{\text{QE}}$ ) are nothing but the width of the state  $|2\rangle$ . Therefore, when the linewidth ( $\Gamma_{\text{SP}}, \Gamma_{\text{DDI}}^{\text{QE}}$ ) of the state  $|2\rangle$  is almost



equal to the energy difference ( $\varepsilon_{2+} - \varepsilon_{2-}$ ), two states merge to one state, and the splitting disappears. That is why we get two peaks to merge into one peak. The present theory can be used to make nanoswitches by using the present prediction of the merging of two-peaks (ON) into one peak (OFF).

Now, we want to comment on the weak- and strong-coupling limits between the exciton and the DDI-QE field interaction. Let us first define the Rabi frequency (energy) for the DDI-QE field as  $\Omega_{\text{DDI}}^{\text{QE}} = \Omega_P \Gamma_{\text{DDI}}^{\text{QE}}$ . The weak-coupling limit in the literature is defined as  $\Omega_{\text{DDI}}^{\text{QE}} < \gamma_0$  and on the other hand the strong-coupling limit is defined as  $\Omega_{\text{DDI}}^{\text{QE}} > \gamma_0$  [29]. The expressions for the density-matrix element ( $\rho_{21}$ ) and the PL intensity in Eqs. (38) and (40) are derived for both the weak- and strong-coupling limits. The expressions for  $\rho_{21}$  and the PL intensity can be obtained in the weak-coupling limit from Eqs. (38) and (40) by neglecting the  $\Omega_{\text{DDI}}^{\text{QE}}$  term in the denominator. Therefore, in the weak-coupling limit, the splitting of the PL peak from one peak to two peaks will disappear. Further, in the derivation of SP linewidth and DDI-QE linewidth, we have used the quantum perturbation theory where the exciton coupling with the DDI-QD and DDI-QE fields is in the weak-coupling limit.

Further, we also comment on the effect of the dissipation on the SP linewidth, the DDI-QE linewidth, and PL emission. The effect of dissipation can be included in our theory by adding a decay linewidth  $\gamma_{nm}$  in the photonic quantized energy  $\varepsilon_{nm}$  as  $\varepsilon_{nm} + i\gamma_{nm}$ . Note that the SP and DDI-QE linewidths are a function of the DOS. We found that the DOS calculated in Eq. (27) has a peak at  $\varepsilon_{21} = \varepsilon_{nm}$ . This is because the number of photons occupying localized states is larger than that of the other energy states. In the presence of the dissipation ( $\gamma_{nm}$ ), the heights of the DOS peaks will decrease. This in turn will decrease the values of the SP and DDI-QE linewidths. We have also shown that the expression of PL intensity depends on the SP and DDI-QE linewidths. Hence

the PL intensity will also decrease due to the dissipation in the nanofiber.

## VI. SUMMARY

The effect of the spontaneous emission on the photoluminescence for the photonic nanofiber doped with an ensemble of quantum dots and quantum emitters has been studied. The bound photonic states of the nanofiber are calculated using the transfer-matrix method. We considered that the excited excitons decay spontaneously due to the exciton and the DDI field interaction. Analytical expressions of spontaneous decay linewidths are calculated using the quantum-mechanical perturbation theory. It is found that the decay linewidth is enhanced when the bound photon energy is close to the excited exciton energy. There is also an enhancement in the decay linewidth due to the DDI coupling. An analytical expression of the photoluminescence is found using the density-matrix method in the presence of the DDI coupling. We have predicted that in the strong DDI coupling the peak in the photoluminescence spectrum splits into two peaks. The splitting is due to the creation of the two dressed states. We have shown that when the bound photon energy is close to the exciton energy, two peaks merge into one peak. This is because the spontaneous linewidth is in the same order magnitude as the energy difference between the two dressed states. We also compared our theory with experiments of a nanofiber made of the poly-4-vinylpyridine core and polystyrene cell. The nanofiber is embedded with an ensemble of the CdSe QDs and S101 dye molecules. A good agreement between theory and experiments is found.

## ACKNOWLEDGMENT

M.R.S. is thankful to the Natural Sciences and Engineering Research Council of Canada for a research grant.

- 
- [1] C. Wang, E. Yan, G. Li, Z. Sun, S. Wang, Y. Tong, W. Li, Y. Xin, Z. Huang, and P. Yan, *Synth. Met.* **160**, 1382 (2010).
  - [2] C. Cheng, F. Wang, and X. Cheng, *Opt. Laser Technol.* **122**, 105812 (2020).
  - [3] Z. Zhang, C. Shao, F. Gao, X. Li, and Y. Liu, *J. Colloid Interface Sci.* **347**, 215 (2010).
  - [4] V. Strong, F. J. Uribe-Romo, M. Battson, and R. Kaner, *Small* **8**, 1191 (2012).
  - [5] A. Camposeo, L. Persano, and D. Pisignano, *Macromol. Mater. Eng.* **298**, 487 (2013).
  - [6] A. De SanLuis, Z. Aguirreurreta, L. M. Pardo, A. Perez-Marquez, J. Maudes, N. Murillo, M. Paulis, and J. R. Leiza, *Isr. J. Chem.* **58**, 1347 (2018).
  - [7] A. Fahmi, D. Appelhans, N. Cheval, T. Pietsch, C. Bellmann, N. Gindy, and B. Voit, *Adv. Mater.* **23**, 3289 (2011).
  - [8] A. Camposeo, M. Gaio, M. Moffa, M. Montinaro, M. Castro-Lopez, V. Fasano, R. Sapienza, and D. Pisignano in *Proceedings of the International Society for Optics and Photonics, San Francisco*, edited by C. E. Tabor, F. Kajzar, T. Kaino, Y. Koike (SPIE, San Francisco, 2017), p. 10101.
  - [9] T. Abitbol, J. T. Wilson, and D. G. Gray, *J. Appl. Polym. Sci.* **119**, 803 (2011).
  - [10] C.-Y. Yan, Z.-Q. Fang, A.-M. Tang, W.-Y. Liu, Y. Liu, and H.-Z. Shi, *Cellulose* **25**, 2405 (2018).
  - [11] S. Chaguetmi, F. Mammeri, M. Pasut, S. Nowak, H. Lecoq, P. Decorse, C. Costentin, S. Achour, and S. Ammar, *J. Nanopart. Res.* **15**, 1 (2013).
  - [12] S. Singh, A. Singh, M. Mittal, R. Srivastava, S. Sapra, and B. Nandan, *Phys. Chem. Chem. Phys.* **21**, 16137 (2019).
  - [13] R. D. Artuso and G. W. Bryant, *Phys. Rev. B* **82**, 195419 (2010).
  - [14] M. Wersäll, J. Cuadra, T. J. Antosiewicz, S. Balci, and T. Shegai, *Nano Lett.* **17**, 551 (2016).
  - [15] B. D. Fainberg, N. N. Rosanov, and N. A. Veretenov, *Appl. Phys. Lett.* **110**, 203301 (2017).
  - [16] Y. Suganuma, P. E. Trudeau, B. Leathem, B. Shieh, and A. Dhirani, *J. Chem. Phys.* **118**, 9769 (2003).

- [17] A. F. Terzis, S. G. Kosionis, J. Boviatsis, and E. Paspalakis, *J. Mod. Optics* **63**, 451 (2016).
- [18] M. R. Singh, *Nanotechnology* **24**, 125701 (2013).
- [19] M. R. Singh, M. Chandra Sekhar, S. Balakrishnan, and S. Masood, *J. Appl. Phys.* **122**, 034306 (2017).
- [20] M. R. Singh, J. D. Cox, and M. Brzozowski, *J. Phys. D* **47**, 085101 (2014).
- [21] A. Franceschetti and A. Zunger, *Appl. Phys. Lett.* **76**, 1731 (2000).
- [22] S. V. Baieva, T. K. Hakala, and J. J. Toppari, *Nanoscale Res. Lett.* **7**, 1 (2012).
- [23] S. Ishizaka, K. Nakatani, S. Habuchi, and N. Kitamura, *Anal. Chem.* **71**, 419 (1999).
- [24] K. Okamoto, *Fundamentals of Optical Waveguides* (Elsevier, New York, 2006), Chap. 2.
- [25] M. J. Adam, *An Introduction to Optical Wave Guide* (Wiley, New York, 1981).
- [26] M. R. Singh and K. Black, *J. Phys. Chem. C* **122**, 26584 (2018).
- [27] L. Novotny and B. Hecht, *Principles of Nano-Optics* (Cambridge University, Cambridge, England, 2006), Sec. 8.3.3, p. 266.
- [28] D. Sarid and W. A. Challener, *Modern Introduction to Surface Plasmons: Theory, Mathematica Modeling, and Applications* (Cambridge University, Cambridge, England, 2010).
- [29] M. O'Scullly and M. Zubairy, *Quantum Optics* (Cambridge University, Cambridge, England, 1997).
- [30] E. Hamura, Y. Kawabe, and A. Yamanaka, *Quantum Nonlinear Optics* (Springer, New York, 2007), Chap. 6.